Received 2 June 2023; revised 17 August 2023; accepted 26 September 2023. Date of publication 29 September 2023; date of current version 16 October 2023.
The review of this article was arranged by Editor M. J. Kumar.

Digital Object Identifier 10.1109/JEDS.2023.3320580

An ASM-HEMT for Large-Signal Modeling of GaN HEMTs in High-Temperature Applications

NICHOLAS C. MILLER[1] (Senior Member, IEEE), ALEXIS BROWN[2], MICHAEL ELLIOTT[3], RYAN GILBERT[3], DEVIN T. DAVIS[3], AHMAD E. ISLAM[1] (Senior Member, IEEE), DENNIS WALKER Jr.[1] (Member, IEEE), GARY HUGHES[1] (Member, IEEE), KYLE LIDDY[1] (Member, IEEE), AND KELSON D. CHABAK[1] (Senior Member, IEEE)

1 Air Force Research Laboratory Sensors Directorate, Wright-Patterson AFB, OH 45433, USA
2 Ardent, Wright-Patterson AFB, OH 45433, USA
3 KBR, Inc., Wright-Patterson AFB, OH 45433, USA

CORRESPONDING AUTHOR: N. C. MILLER (e-mail: ncmiller@ieee.org)

This work was supported by the Air Force Research Laboratory under Award FA807518D0015.

ABSTRACT This paper reports a temperature-dependent ASM-HEMT for modeling GaN HEMTs at elevated temperatures. Modifications to the standard ASM-HEMT were developed to accurately capture the DC and RF measurements collected at varying chuck temperatures. Several results are reported which validate the model including DC-IV, pulsed-IV, scattering-parameter, and load-pull measurements. The model is then used to extrapolate the performance of the GaN HEMT to twice the operating temperature at which the model was validated. This work could be useful for understanding and modeling GaN HEMTs in high-temperature environment applications.

INDEX TERMS Gallium nitride, high electron mobility transistor, high temperature, ASM-HEMT, load pull.

I. INTRODUCTION

Design and rigorous analysis of high-temperature electronics is becoming an increasingly important topic. Applications including hypersonic vehicles and deep oil drilling present significantly demanding requirements for semiconductor technologies [1]. Gallium nitride (GaN) high electron mobility transistors (HEMTs) are a promising compound semiconductor technology for radio frequency (RF) power amplifier (PA) and low noise amplifier integrated circuits in extreme environments [2], [3]. Thorough understanding and accurate modeling of state-of-the-art GaN HEMTs at elevated temperatures is paramount for first pass design success of integrated circuits.

An important aspect of the high-temperature integrated circuit design process is the characterization of the GaN HEMTs at elevated temperatures. There are various characterization studies of the transistors in the literature. In [4], the large-signal response of a packaged GaN HEMT was characterized at channel temperatures near 350°C. Tan et al. reported high-temperature DC performance of AlGaN/GaN HEMTs on silicon substrates up to 500°C in [5]. A study of high-temperature DC performance of GaN HEMTs on silicon and sapphire substrates up to 350°C was reported in [6]. The DC and large-signal response of InAlN/GaN HEMTs at elevated temperatures ranging from 600 – 900°C was reported by Maier et al. in [7], [8].

Small-signal modeling of GaN HEMTs at elevated temperatures has been extensively studied in the literature. Crupi et al. reported on the temperature influence of GaN HEMT equivalent circuits up to 80°C in [9]. The small-signal model parameters of a GaN HEMT were analyzed over a range of temperatures up to 150°C in [10]. A high periphery GaN HEMT was modeled up to 200°C in [11]. Neural networks have also been employed for temperature-dependent small-signal modeling in [12], [13].

Nonlinear and large-signal compact modeling is an important aspect of PA circuit design for high-temperature applications. Several examples of temperature-dependent large-signal modeling of GaN transistors exist in the literature. Lee and Webb reported on a temperature-dependent Curtice

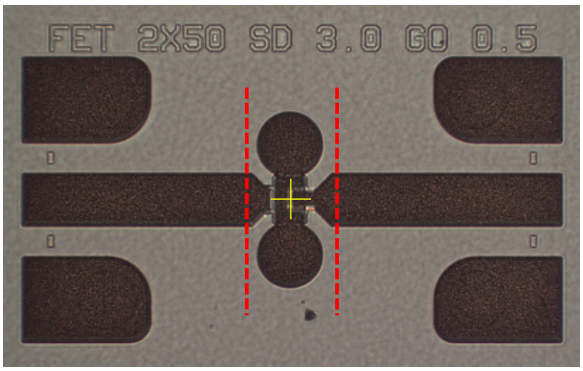

FIGURE 1. Image of the measured and modeled on-wafer unmatched GaN HEMT. The dashed lines represent the reference planes established with the multiline TRL calibration.

model for GaN HEMTs in [14]. A temperature-dependent modified Angelov model was reported in [15]. Deng et al. reported a temperature-dependent Curtice and Angelov model for GaN MOSHFETs in [16] and [17], respectively. Hassan et al. reported a temperature-dependent Angelov model extracted from DC measurements up to 600°C in [18]. Other works on nonlinear temperature-dependent modeling of GaN HEMTs include [19], [20], [21], [22], [23], [24], [25], [26].

Physics-based models have received considerable interest for accurate modeling of GaN HEMTs. The ASM-HEMT is one such physics-based model which has shown promise in the literature [27], [28], [29], [30], [31], [32], [33]. This model has been employed for numerous applications including several recent works on statistical nonlinear modeling [34] and deep learning-based nonlinear modeling [35]. The temperature dependence of GaN HEMTs has also been modeled with the ASM-HEMT. However, this work was limited to DC measurements and modeling [20], [22], [36].

This work presents a temperature-dependent ASM-HEMT validated with on-wafer load-pull measurements collected versus chuck temperature. Section II provides a detailed description of the temperature-dependent model extraction and the modifications required to accurately capture the measured data. In Section III, the well-calibrated ASM-HEMT is then used to project the large-signal performance of the GaN HEMT to twice the operating temperature at which the model was validated. The paper is concluded in Section IV.

II. TEMPERATURE-SCALABLE ASM-HEMT

A temperature-dependent ASM-HEMT was extracted from measurements of a 140 nm gate length GaN HEMT [30]. The measured and modeled transistor was a 2x50μm GaN HEMT illustrated in Fig. 1. On-wafer measurements were collected on a probe station with variable chuck (ambient) temperature. DC and scattering-parameter (S-parameter) measurements were collected on a Cascade 12K probe station with an ERS Electronic GmbH Aircool SP72-T2 chuck temperature controller. An 8 – 50 GHz vector-receiver load-pull test

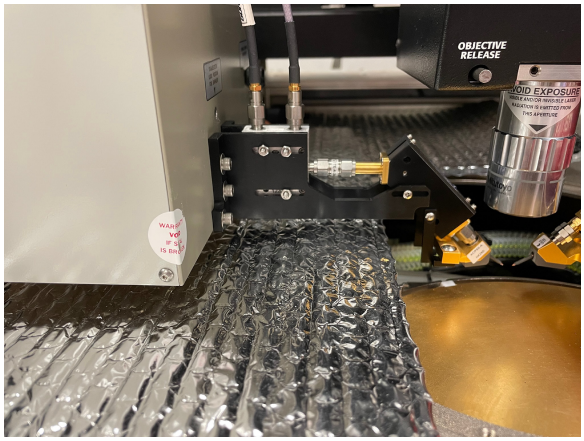

FIGURE 2. On-wafer vector-receiver load-pull measurement system with temperature controllable chuck. Custom heat shielding was employed to protect sensitive system components from heat radiation.

bench was employed for model verification versus ambient temperature. Fig. 2 reports a photo of the on-wafer vector-receiver load-pull system. The on-wafer RF measurements were calibrated using the multiline thru-reflect-line (TRL) algorithm [37]. No trap model was employed in this work.

A. DC MODEL

The DC parameters of the ASM-HEMT were first extracted from room temperature measurements of the GaN HEMT in a fashion similar to [30], [31], [32]. The model was verified by analyzing the DC drain current versus gate voltage and the calculated transconductance at a drain supply voltage of $V_{DS} = 10$ V. Next, the DC model was finalized by tuning parameters to fit the room temperature pulsed-IV (PIV) measurements of the GaN HEMT following the modeling approach in [38].

Next, the temperature dependence of the ASM-HEMT was analyzed by comparing the model to on-wafer measurements collected at varying chuck temperatures. The "*tnom*" parameter was varied to affect the temperature-dependent parameters in the ASM-HEMT [36], and was set equal to a newly defined sweep parameter T_{amb}. Several parameters of the temperature-dependent model were adjusted in an attempt to accurately capture the measured DC-IV data. However, the standard ASM-HEMT temperature dependence was found to be insufficient for accurately capturing the temperature-dependent DC measurements. The ASM-HEMT was modified by prescribing linear functions to two key parameters in order to fit the measurements. These parameters were the threshold voltage, *voff*, and the sub-threshold slope variation due to drain voltage, *cdscd*. The modifications to the standard ASM-HEMT parameters were

$$voff = -2.92 + (T_{amb} - 25) \cdot 1.933 \times 10^{-3}, \quad (1)$$

$$cdscd = 0.051 + (T_{amb} - 25) \cdot 1.593 \times 10^{-3}. \quad (2)$$

Here, the y-intercepts of the linear equations represent the parameter values extracted at 25°C and the slopes represent

TABLE 1. Summary of key temperature parameters.

Parameter	Corresponding parameter	Extracted Value
ute	low field mobility (u0)	-0.55
kt1	threshold voltage (voff)	-0.3
kns0	2-DEG charge density at access region	0.24
utes	mobility in source access region (u0accs)	1.67
uted	mobility in drain access region (u0accd)	2.5

the parameter rates of change with respect to the ambient temperature referenced to 25°C. A summary of the key ASM-HEMT temperature parameters are reported in Table 1. The combination of parameters outlined in the table and the two modified parameters provided a temperature-scalable DC ASM-HEMT.

Validations of the temperature-scalable ASM-HEMT were analyzed by comparing model results against DC measurements collected at ambient temperatures ranging from 25°C to 175°C with 50°C steps. The DC drain current and transconductance at a quiescent drain supply voltage of V_{DS} =10 V were used for these purposes. Fig. 3 illustrates the measured (solid lines) and simulated (dashed lines) data at the various ambient temperatures. The DC transconductance measurements (solid lines) and simulations (dashed lines) are reported in Fig. 4. Both figures indicate good agreement between the temperature-scalable ASM-HEMT and the DC measurements.

The trend in threshold voltage and sub-threshold slope variation due to drain voltage versus ambient temperature are most apparent in the DC transconductance measurements illustrated in Fig. 4. These changes in the device currents with respect to the ambient temperature are attributed to the electron Fermi levels accessing higher energy levels due to increased electron temperatures. The broadening of the Fermi distributions allow for more buffer leakage at higher ambient temperatures. Both the threshold voltage and sub-threshold slope variation due to drain voltage increase as the ambient temperature increases. This is accurately captured in the model using the combination of the negative *ute* parameter value outlined in Table 1 and the modified ASM-HEMT parameters in Eqs. (1) and (2). The results in Figs. 3 and 4 indicate bias conditions for which drain current and transconductance are insensitive to temperature. These zero-temperature coefficients are also inherent in different field effect transistor technologies [39], [40].

Following the practice outlined in [30], [38], the ASM-HEMT simulations were compared to measured PIV data collected at the four different ambient temperatures. The PIV measurements were collected using a quiescent bias of V_{DS} = 10 V and I_D = 100 mA/mm. Fig. 5 reports the measured PIV data (solid lines) and the simulated IV data (dashed lines) of the GaN HEMT. Although the trend in measured PIV data versus ambient temperature is captured, there are several discrepancies in the simulated IV data. Most notably, the measured knee voltage and on-resistance are not perfectly captured with the ASM-HEMT simulations. Average errors of the simulated IV data are 4%, 2.6%, 2%, and 3.2% at 25°C, 75°C, 125°C, and 175°C, respectively. These modest errors were found to be sufficient for the overall temperature-scalable nonlinear ASM-HEMT.

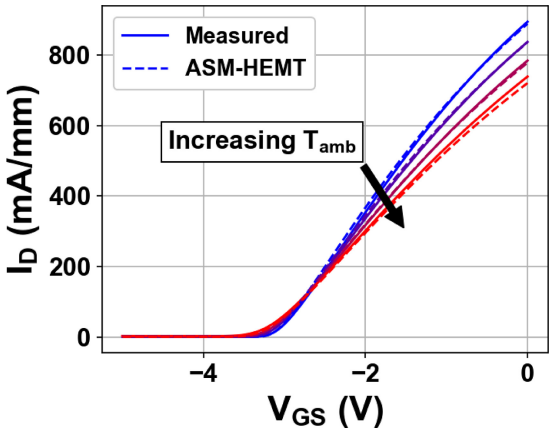

FIGURE 3. Measured (solid lines) and simulated (dashed lines) drain current versus gate supply voltage of the GaN HEMT at ambient temperatures ranging from 25°C to 175°C with 50°C steps.

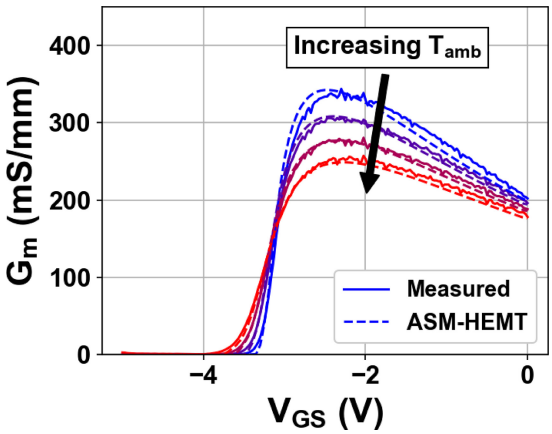

FIGURE 4. Measured (solid lines) and simulated (dashed lines) DC transconductance versus gate supply voltage of the GaN HEMT at ambient temperatures ranging from 25°C to 175°C with 50°C steps.

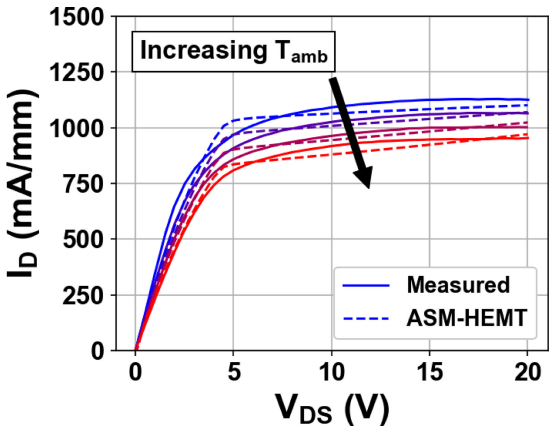

FIGURE 5. Measured PIV (solid lines) and simulated IV (dashed lines) of the GaN HEMT at ambient temperatures ranging from 25°C to 175°C with 50°C steps.

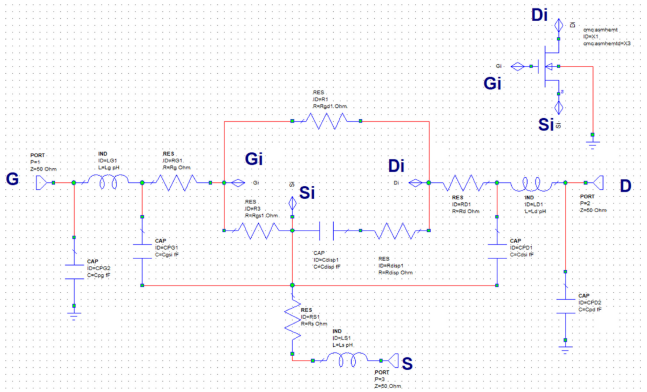

FIGURE 6. Circuit topology of the ASM-HEMT connected to an extrinsic parasitic network.

B. RF MODEL

After extraction and validation of the core DC ASM-HEMT, the RF model was next investigated. First, the extrinsic parasitic network was extracted at room temperature following the well-known cold field effect transistor (FET) procedure. This work employs the extrinsic parasitic network outlined in [41] which is wrapped around the core ASM-HEMT. The ASM-HEMT with the chosen extrinsic parasitic network is reported in Fig. 6. The remaining key parameters which required tuning for good agreement with S-Parameter measurements collected at 25°C were the "*cgso*", "*cgdo*", and "*cdso*" parameters [28], [33]. The ASM-HEMT S-Parameter simulations were then compared to measurements at increasing ambient temperatures. However, the standard model extracted from room temperature measurements was again found to be insufficient for accurately capturing the measured S-Parameters versus ambient temperature. This work employed modifications to the three capacitance parameters to accurately fit the measurements. Furthermore, the extrinsic gate resistance parasitic parameter was also modified based on cold FET measurements collected at the increasing ambient temperatures. The linear functions prescribed to the four RF parameters were

$$cgso = [82 - (\mathrm{T_{amb}} - 25) \cdot 0.173] \times 10^{-15}, \quad (3)$$

$$cgdo = [13.6 + (\mathrm{T_{amb}} - 25) \cdot 0.036] \times 10^{-15}, \quad (4)$$

$$cdso = [17.5 + (\mathrm{T_{amb}} - 25) \cdot 0.048] \times 10^{-15}, \quad (5)$$

$$Rg = 3.2 + (\mathrm{T_{amb}} - 25) \cdot 18.6 \times 10^{-3}. \quad (6)$$

Similar to the modified DC parameters, the y-intercepts of the modified RF parameters represent the values extracted from measurements collected at 25°C. The slopes of the linear functions were extracted to fit measurements across the range of ambient temperatures.

Comparisons of the measured S-Parameters and ASM-HEMT simulations from 0.5 – 40 GHz and across a range of ambient temperatures were next analyzed. The chuck temperature of the S-Parameter measurement bench was elevated from 25°C to 175°C in 50°C steps. The S-Parameters were measured and simulated at the quiescent bias of $V_{DS} = 10\,\mathrm{V}$ and $I_D = 100\,\mathrm{mA/mm}$. Fig. 7 illustrates the measured (solid lines) and ASM-HEMT simulated (dashed lines) S-Parameters of the GaN HEMT across the range of ambient temperatures. The measured and ASM-HEMT simulated h_{21} and maximum small-signal gain, $\mathrm{G_{max}}$, are reported in Fig. 8 and Fig. 9, respectively. Both figures indicate a good agreement between the S-Parameter measurements and the equivalent small-signal simulations. A summary of the ASM-HEMT small-signal simulation errors versus ambient temperature are reported in Table 2.

Here, the errors of ASM-HEMT simulated S-Parameters are averaged over frequency at each ambient temperature. These results exhibit modest errors with a maximum of 11.7% in S_{12} at 25°C. The results also indicate that the temperature-scalable ASM-HEMT provides good prediction of $\mathrm{G_{max}}$ values computed from S-Parameter measurements

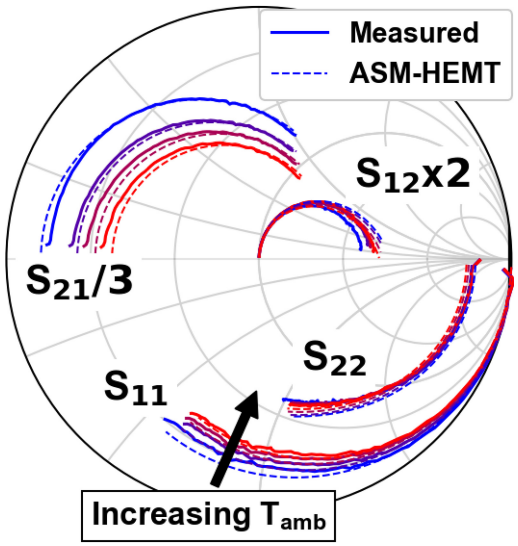

FIGURE 7. Measured (solid lines) and simulated (dashed lines) S_{11}, S_{21}, S_{12}, and S_{22} of the GaN HEMT at ambient temperatures ranging from 25°C to 175°C with 50°C steps.

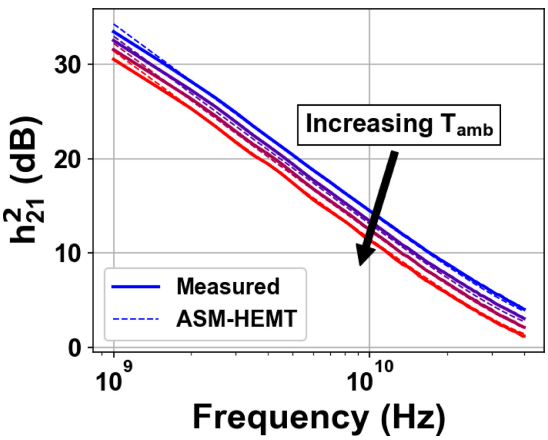

FIGURE 8. Measured (solid lines) and simulated (dashed lines) h_{21} of the GaN HEMT at ambient temperatures ranging from 25°C to 175°C with 50°C steps.

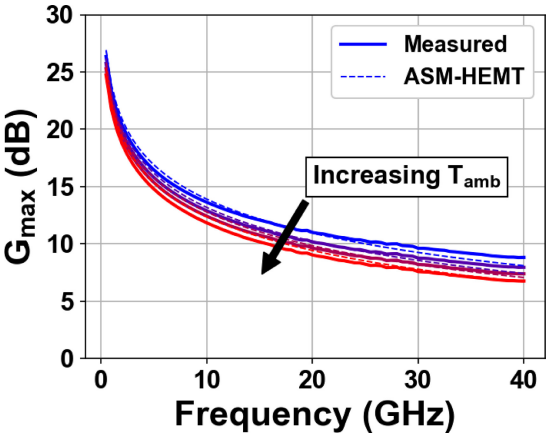

FIGURE 9. Measured (solid lines) and simulated (dashed lines) G_{max} of the GaN HEMT at ambient temperatures ranging from 25°C to 175°C with 50°C steps.

TABLE 2. Errors of small-signal model simulations.

T_{amb} (°C)	S_{11} (%)	S_{12} (%)	S_{21} (%)	S_{22} (%)
25	3.8	11.7	2.6	9.4
75	2.5	8.0	1.9	5.4
125	3.8	7.9	3.0	4.2
175	5.6	9.2	5.0	4.1

at the various chuck temperatures. This capability could be useful for future investigations of GaN HEMT performance in high temperature environments.

Finally, large-signal simulations of the temperature-scalable ASM-HEMT were compared to temperature-dependent on-wafer vector-receiver power measurements of the GaN HEMT. It is noted that the "*Rsub*" parameter reported in [28] was used to accurately capture the measured power added efficiency (PAE) at room temperature. Furthermore, this parameter was modified with a linear function,

$$Rsub = 10000 + (T_{amb} - 25) \cdot 2821, \tag{7}$$

to accurately capture the measured PAE versus chuck temperature.

Power-sweep measurements of the GaN HEMT were collected on-wafer using a Ka-band vector-receiver load-pull test bench. All measurements of the GaN HEMT were collected at a 30 GHz fundamental frequency and a quiescent bias of V_{DS} = 10 V and I_D =100 mA/mm. The load impedance was prescribed for optimal PAE within the limits of the passive vector-receiver measurement system. Fig. 10 reports a comparison of the measured (solid lines) and ASM-HEMT simulated (dashed lines with circle markers) output power versus available input power. Figs. 11 and 12 report the comparisons between measured and ASM-HEMT simulated power gain and PAE, respectively. The results in Figs. 10–12 indicate good agreement between the ASM-HEMT large-signal simulations and the temperature-dependent power-sweep measurements of the GaN HEMT. A summary of the ASM-HEMT large-signal

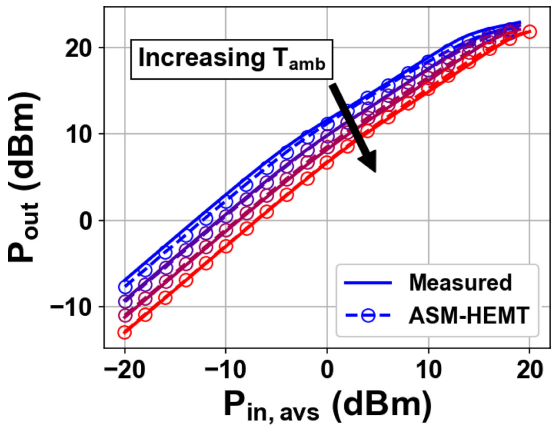

FIGURE 10. Measured (solid lines) and simulated (dashed lines with circle markers) output power of the GaN HEMT versus available input power at ambient temperatures ranging from 25°C to 175°C with 50°C steps.

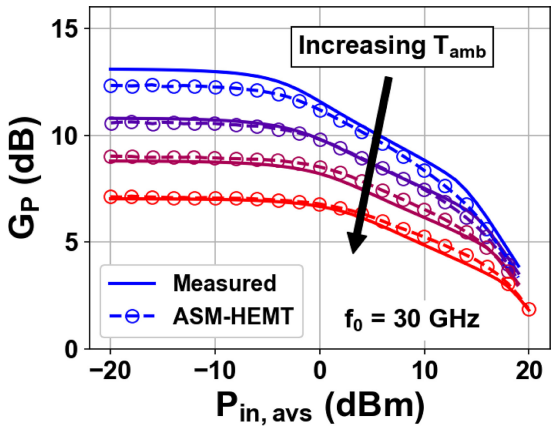

FIGURE 11. Measured (solid lines) and simulated (dashed lines with circle markers) power gain of the GaN HEMT versus available input power at ambient temperatures ranging from 25°C to 175°C with 50°C steps.

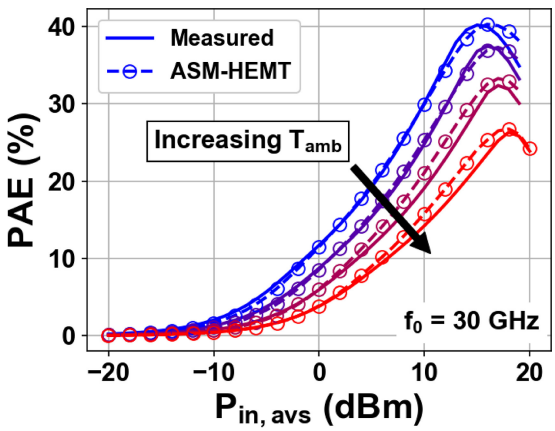

FIGURE 12. Measured (solid lines) and simulated (dashed lines with circle markers) PAE of the GaN HEMT versus available input power at ambient temperatures ranging from 25°C to 175°C with 50°C steps.

simulation errors is reported in Table 3. The errors were computed as the relative difference in ASM-HEMT simulations compared to the measurements at peak available input power. Modest errors in the large-signal ASM-HEMT

TABLE 3. Errors of large-signal model simulations.

T_{amb} (°C)	P_{out} (%)	G_P (%)	PAE (%)
25	2.4	13.9	9.3
75	1.5	9.2	7.2
125	0.6	4.0	5.5
175	0.1	3.8	1.5

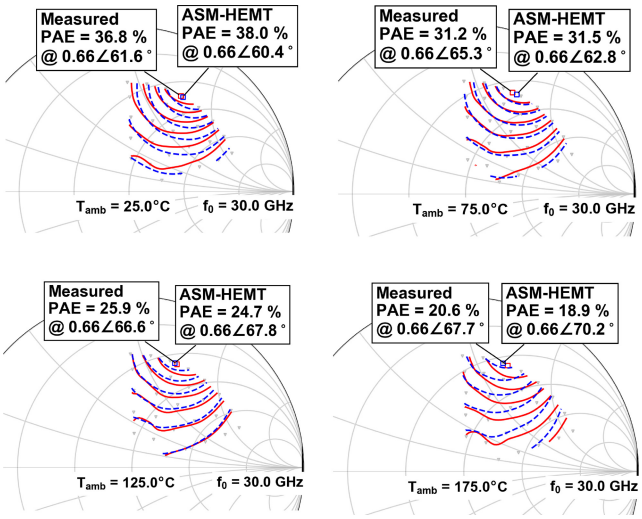

FIGURE 13. Measured (solid red lines) and ASM-HEMT simulated (dashed blue lines) PAE contours of the GaN HEMT at 30 GHz, $P_{in,avs}$ = 11 dBm, and at 25°C (top left), 75°C (top right), 125°C (bottom left), and 175°C (bottom right).

simulations are reported, with the highest error observed in power gain at 25°C. However, the errors decrease as the ambient temperature increases. This provides confidence in the temperature-scalable large-signal ASM-HEMT validated at a single Ka-band frequency.

Finally, load-pull measurements and simulations were analyzed. The on-wafer vector-receiver load-pull bench was again employed for these purposes at a 30 GHz fundamental frequency. The transistor was biased at $V_{DS} = 10$ V and I_D =100 mA/mm. Fig. 13 illustrates the measured and ASM-HEMT simulated PAE contours. Ambient temperatures of 25°C, 75°C, 125°C, and 175°C were used for the data in the top left, top right, bottom left, and bottom right, respectively. The average absolute error between the load-pull PAE measurements and the ASM-HEMT simulations are 1.6%, 0.6%, 0.5%, and 1.1% at the 25°C, 75°C, 125°C, and 175°C ambient temperatures, respectively. These results indicate a good agreement between the temperature-scalable ASM-HEMT and the measured load-pull data. This provides confidence in the ASM-HEMT's ability to optimize the transistor performance in operating conditions beyond where the GaN HEMT was measured.

III. MODEL PROJECTIONS AT 350°C

Depending on the application, GaN HEMTs can likely operate at ambient temperatures which are considerably higher than what can be tested on today's on-wafer RF measurement systems. This poses considerable challenges for

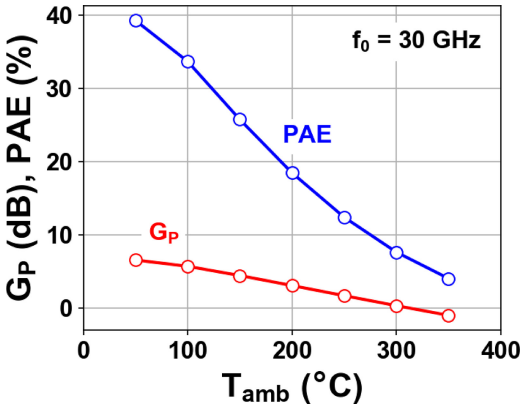

FIGURE 14. Simulated power gain (red) and PAE (blue) versus ambient temperature of the GaN HEMT at 30 GHz and $P_{in,avs}$ = 15 dBm.

RF engineers who must design integrated circuits without measured data. This work considers extrapolation of the temperature-dependent ASM-HEMT in order to provide model projections at ambient temperatures beyond what can be measured on wafer. To this end, the ASM-HEMT was extrapolated to 350°C – twice the highest ambient temperature at which the model was validated.

Simulated large-signal projections were first analyzed by sweeping the ambient temperature of the ASM-HEMT from 50°C to 350°C with 50°C steps while maintaining a fixed load impedance. The resulting power gain and PAE at 15 dBm available input power versus ambient temperature are illustrated in Fig. 14. This data indicates the severe degradation of the GaN HEMT's Ka-band large-signal performance at elevated ambient temperatures. The GaN HEMT's large-signal power gain drops from 6.6 dB at 50°C operating temperature to −0.9 dB at 350°C operating temperature. Furthermore, the transistor PAE drops from 39.3% at 50°C operating temperature to 4% at 350°C operating temperature. It is clear from these large-signal simulations that the 140 nm GaN HEMT must be optimized to increase its Ka-band power performance at the chosen 350°C operating temperature.

In an attempt to optimize the transistor performance at 350°C, load-pull simulations of the temperature-scalable ASM-HEMT were next analyzed to provide understanding of the model's response to loading conditions at elevated temperatures. First, load pull of the ASM-HEMT was simulated at 25°C to set a baseline understanding of the load impedance space. Then, the ASM-HEMT was load pulled at the 350°C operating temperature. Fig. 15 compares the simulated PAE contours at 25°C and 350°C. Here, the dashed blue lines illustrate the simulated PAE contours at 25°C and the solid red lines illustrate the simulated PAE contours at 350°C. There is a clear shift in the optimal load impedance for maximum PAE that can be exploited to increase the transistor performance at 350°C.

A simulated power sweep of the temperature-scalable ASM-HEMT at 350°C was next collected at the optimal

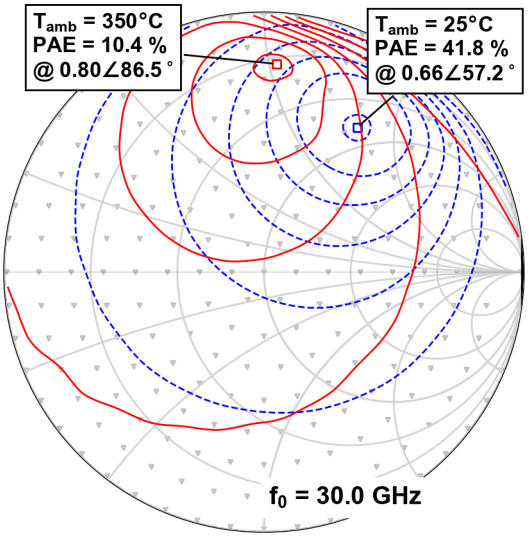

FIGURE 15. Simulated PAE contours of the GaN HEMT at 30 GHz, $P_{in,avs}$ = 15 dBm, and at 25°C (dashed blue lines) and 350°C (solid red lines) operating temperatures.

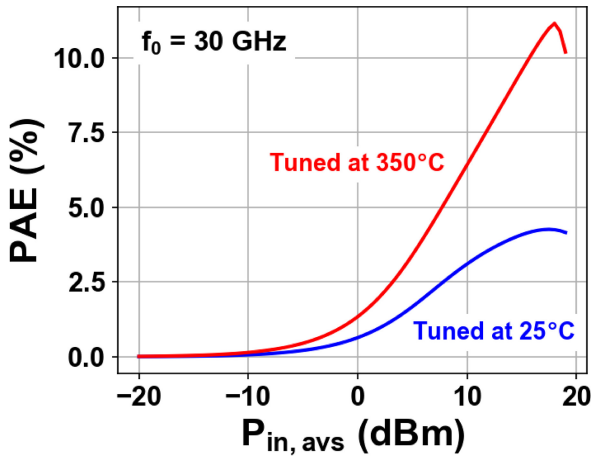

FIGURE 16. Simulated PAE of the GaN HEMT versus available input power at 30 GHz and using the load impedance determined at 25°C (blue) and the load impedance optimized at 350°C (red).

load impedance determined from the load-pull simulations at 350°C. Fig. 16 illustrates the ASM-HEMT power-sweep simulations using the load impedance determined from the 25°C measurements (blue) and the 350°C optimized load impedance (red). Here, the peak PAE using the 25°C load impedance was 4.2% and the peak PAE using the 350°C load impedance was 11.1%. The temperature-scalable ASM-HEMT simulations indicate that re-tuning the transistor based on high-temperature load pull can boost the PAE by 7 percentage points. The temperature-dependent simulations also provide RF design engineers projected guidelines for how optimal load impedances may shift in high temperature environments. In this case, the GaN HEMT's optimal load reflection coefficient at a 350°C operating temperature shifted by 0.14 in magnitude and nearly 30 degrees phase compared to the GaN HEMT's optimal load reflection coefficient at room temperature.

IV. CONCLUSION

This work reported a temperature-scalable ASM-HEMT for Ka-band large-signal modeling of GaN HEMTs at elevated temperatures. The standard model found in commercial design software was found to be insufficient for accurately capturing the temperature-dependent measurements. Several modifications to the ASM-HEMT parameters were reported. The resulting model was extracted and validated with DC-IV, PIV, and S-Parameter measurements at various ambient temperatures. The large-signal performance of the ASM-HEMT was then validated with on-wafer load-pull measurements at varying ambient temperatures. Finally, the model was used to project the performance of the GaN HEMT at a 350°C operating temperature. It was found that the GaN HEMT's large-signal Ka-band performance severely degraded at this operating temperature, and load-pull simulations were required to optimize transistor performance. This work could be useful for future GaN HEMT modeling and design for high temperature environment applications.

REFERENCES

[1] J. Watson and G. Castro, "A review of high-temperature electronics technology and applications," *J. Mater. Sci. Mater. Electron.*, vol. 26, pp. 9226–9235, Jul. 2015, doi: 10.1007/s10854-015-3459-4.
[2] M. Yuan et al., "GaN ring oscillators operational at 500°C based on a GaN-on-Si platform," *IEEE Electron Device Lett.*, vol. 43, no. 11, pp. 1842–1845, Nov. 2022, doi: 10.1109/LED.2022.3204566.
[3] P. Neudeck, R. Okojie, and L.-Y. Chen, "High-temperature electronics—A role for wide bandgap semiconductors?" *Proc. IEEE*, vol. 90, no. 6, pp. 1065–1076, Jun. 2002, doi: 10.1109/JPROC.2002.1021571.
[4] N. Adachi, Y. Tateno, S. Mizuno, A. Kawano, J. Nikaido, and S. Sano, "High temperature operation of AlGaN/GaN HEMT," in *IEEE MTT-S Int. Microw. Symp. Dig.*, 2005, pp. 507–510, doi: 10.1109/MWSYM.2005.1516642,
[5] W. S. Tan, M. J. Uren, P. W. Fry, P. A. Houston, R. S. Balmer, and T. Martin, "High temperature performance of AlGaN/GaN HEMTs on Si substrates," *Solid-State Electron.*, vol. 50, no. 3, pp. 511–513, 2006, doi: 10.1016/j.sse.2006.02.008.
[6] R. Cuerdo et al., "High temperature behaviour of GaN HEMT devices on Si(111) and sapphire substrates," *Physica Status Solidi c*, vol. 5, no. 6, pp. 1971–1973, 2008, doi: 10.1002/pssc.200778555.
[7] D. Maier et al., "Testing the temperature limits of GaN-based HEMT devices," *IEEE Trans. Device Mater. Rel.*, vol. 10, no. 4, pp. 427–436, Dec. 2010, doi: 10.1109/TDMR.2010.2072507.
[8] D. Maier et al., "InAlN/GaN HEMTs for operation in the 1000°C regime: A first experiment," *IEEE Electron Device Lett.*, vol. 33, no. 7, pp. 985–987, Jul. 2012, doi: 10.1109/LED.2012.2196972.
[9] G. Crupi, A. Raffo, G. Avolio, D. M. M.-P. Schreurs, G. Vannini, and A. Caddemi, "Temperature influence on GaN HEMT equivalent circuit," *IEEE Microw. Wireless Compon. Lett.*, vol. 26, no. 10, pp. 813–815, Oct. 2016, doi: 10.1109/LMWC.2016.2601487.
[10] M. A. Alim, A. A. Rezazadeh, and C. Gaquiere, "Small signal model parameters analysis of GaN and GaAs based HEMTs over temperature for microwave applications," *Solid-state Electron.*, vol. 119, pp. 11–18, May 2016, doi: 10.1016/j.sse.2016.02.002.
[11] G. Crupi, A. Raffo, V. Vadalà, G. Vannini, and A. Caddemi, "High-periphery GaN HEMT modeling up to 65 GHz and 200°C," *Solid-State Electron.*, vol. 152, pp. 11–16, Feb. 2019, doi: 10.1016/j.sse.2018.11.006.
[12] A. Jarndal, S. Husain, and M. Hashmi, "On temperature-dependent small-signal modelling of GaN HEMTs using artificial neural networks and support vector regression," *IET Microw., Antennas Propagat.*, vol. 15, no. 8, pp. 937–953, 2021, doi: 10.1049/mia2.12112.

[13] Z. Marinković et al., "Neural approach for temperature-dependent modeling of GaN HEMTs," *Int. J. Numer. Model. Electron. Netw., Devices Fields*, vol. 28, no. 4, pp. 359–370, 2015, doi: 10.1002/jnm.2011.

[14] J.-W. Lee and K. J. Webb, "A temperature-dependent nonlinear analytic model for AlGaN-GaN HEMTs on SiC," *IEEE Trans. Microw. Theory Techn.*, vol. 52, no. 1, pp. 2–9, Jan. 2004, doi: 10.1109/TMTT.2003.821227.

[15] C. Wang et al., "An electrothermal model for empirical large-signal modeling of AlGaN/GaN HEMTs including self-heating and ambient temperature effects," *IEEE Trans. Microw. Theory Techn.*, vol. 62, no. 12, pp. 2878–2887, Dec. 2014, doi: 10.1109/TMTT.2014.2364821.

[16] J. Deng et al., "RF large-signal model for SiO2/AlGaN/GaN MOSHFETs," in *Proc. IEEE MTT-S Int. Microw. Symp. Dig.*, 2008, pp. 1417–1420, doi: 10.1109/MWSYM.2008.4633044.

[17] J. Deng et al., "Temperature-dependent RF large-signal model of GaN-based MOSHFETs," *IEEE Trans. Microw. Theory Techn.*, vol. 56, no. 12, pp. 2709–2716, Dec. 2008, doi: 10.1109/TMTT.2008.2007083.

[18] A. Hassan, M. Amer, Y. Savaria, and M. Sawan, "Towards GaN500-based high temperature ICs: Characterization and modeling up to 600°C," in *Proc. 18th IEEE Int. New Circuits Syst. Conf. (NEWCAS)*, 2020, pp. 275–278, doi: 10.1109/NEWCAS49341.2020.9159796.

[19] M. Huque, S. Eliza, T. Rahman, H. Huq, and S. Islam, "Temperature dependent analytical model for current–voltage characteristics of AlGaN/GaN power HEMT," *Solid-State Electron.*, vol. 53, no. 3, pp. 341–348, 2009, doi: 10.1016/j.sse.2009.01.004.

[20] S. Ghosh, S. A. Ahsan, Y. S. Chauhan, and S. Khandelwal, "Modeling of source/drain access resistances and their temperature dependence in GaN HEMTs," in *Proc. IEEE Int. Conf. Electron Devices Solid-State Circuits (EDSSC)*, 2016, pp. 247–250, doi: 10.1109/EDSSC.2016.7785254.

[21] X. Zhao et al., "Temperature-dependent access resistances in large-signal modeling of Millimeter-wave AlGaN/GaN HEMTs," *IEEE Trans. Microw. Theory Techn.*, vol. 65, no. 7, pp. 2271–2278, Jul. 2017, doi: 10.1109/TMTT.2017.2658561.

[22] S. A. Albahrani et al., "Extreme temperature modeling of AlGaN/GaN HEMTs," *IEEE Trans. Electron Devices*, vol. 67, no. 2, pp. 430–437, Feb. 2020, doi: 10.1109/TED.2019.2960573.

[23] H. Luo, Z. Zhong, W. Hu, and Y. Guo, "Analysis and modeling of the temperature-dependent nonlinearity of intrinsic capacitances in AlGaN/GaN HEMTs," *IEEE Microw. Wireless Compon. Lett.*, vol. 31, no. 4, pp. 373–376, Apr. 2021, doi: 10.1109/LMWC.2021.3057444.

[24] M. S. Nazir, P. Kushwaha, A. Pampori, S. A. Ahsan, and Y. S. Chauhan, "Electrical characterization and modeling of GaN HEMTs at cryogenic temperatures," *IEEE Trans. Electron Devices*, vol. 69, no. 11, pp. 6016–6022, Nov. 2022, doi: 10.1109/TED.2022.3204523.

[25] N. Sahebghalam, M. Shalchian, A. Chalechale, and F. Jazaeri, "High-temperature HEMT model," *IEEE Trans. Electron Devices*, vol. 69, no. 9, pp. 4821–4827, Sep. 2022, doi: 10.1109/TED.2022.3184662.

[26] J. Yang and J. Zhu, "An extended-temperature IV model for GaN HEMTs," *Solid-State Electron.*, vol. 194, Aug. 2022, Art. no. 108389, doi: 10.1016/j.sse.2022.108389.

[27] S. Khandelwal et al., "ASM GaN: Industry standard model for GaN RF and power devices—Part 1: DC, CV, and RF model," *IEEE Trans. Electron Devices*, vol. 66, no. 1, pp. 80–86, Jan. 2019, doi: 10.1109/TED.2018.2867874.

[28] S. A. Ahsan, S. Ghosh, S. Khandelwal, and Y. S. Chauhan, "Physics-based multi-bias RF large-signal GaN HEMT modeling and parameter extraction flow," *IEEE J. Electron Devices Soc.*, vol. 5, no. 5, pp. 310–319, Sep. 2017, doi: 10.1109/JEDS.2017.2724839.

[29] J. Hodges, S. A. Albahrani, B. Schwitter, and S. Khandelwal, "Accurate non-linear large signal physics-based modeling for Ka-band GaN power amplifier design with ASM-HEMT," in *Proc. IEEE MTT-S Int. Microw. Symp. (IMS)*, 2021, pp. 349–351, doi: 10.1109/IMS19712.2021.9574979.

[30] N. C. Miller et al., "Accurate nonlinear GaN HEMT simulations from X- to Ka-band using a single ASM-HEMT model," in *Proc. IEEE 21st Annu. Wireless Microw. Technol. Conf. (WAMICON)*, 2021, pp. 1–4, doi: 10.1109/WAMICON47156.2021.9615166.

[31] N. C. Miller et al., "Accurate non-linear harmonic simulations at X-band using the ASM-HEMT model validated with NVNA measurements," in *Proc. IEEE Topical Conf. RF/Microw. Power Amplifiers Radio Wireless Appl. (PAWR)*, 2022, pp. 11–13, doi: 10.1109/PAWR53092.2022.9719743.

[32] N. C. Miller, M. Elliott, R. Gilbert, E. Arkun, and D. J. Denninghoff, "Surmounting W-band scalar load-pull limitations using the ASM-HEMT model for millimeter-wave GaN HEMT technology large-signal assessment," in *Proc. 99th ARFTG Microw. Meas. Conf. (ARFTG)*, 2022, pp. 1–4, doi: 10.1109/ARFTG54656.2022.9896585.

[33] S. Khandelwal, *Advanced SPICE Model for GaN HEMTs (ASM-HEMT): A New Industry-Standard Compact Model for GaN-based Power and RF Circuit Design*. Cham, Switzerland: Springer, 2022.

[34] F. Chavez, N. C. Miller, D. T. Davis, and S. Khandelwal, "Statistical modeling of manufacturing variability in GaN HEMT I-V characteristics with ASM-HEMT," in *Proc. IEEE/MTT-S Int. Microw. Symp.*, 2022, pp. 375–377, doi: 10.1109/IMS37962.2022.9865304.

[35] F. Chavez, D. T. Davis, N. C. Miller, and S. Khandelwal, "Deep learning-based ASM-HEMT I-V parameter extraction," *IEEE Electron Device Lett.*, vol. 43, no. 10, pp. 1633–1636, Oct. 2022, doi: 10.1109/LED.2022.3197800.

[36] S. Ghosh et al., "Modeling of temperature effects in a surface-potential based ASM-HEMT model," in *Proc. IEEE 2nd Int. Conf. Emerg. Electron. (ICEE)*, 2014, pp. 1–4, doi: 10.1109/ICEmElec.2014.7151197.

[37] R. B. Marks, "A multiline method of network analyzer calibration," *IEEE Trans. Microw. Theory Techn.*, vol. 39, no. 7, pp. 1205–1215, Jul. 1991. [Online]. Available: http://ieeexplore.ieee.org/document/85388/

[38] L. Dunleavy, C. Baylis, W. Curtice, and R. Connick, "Modeling GaN: Powerful but challenging," *IEEE Microw. Mag.*, vol. 11, no. 6, pp. 82–96, Oct. 2010, doi: 10.1109/MMM.2010.937735.

[39] A. Caddemi, G. Crupi, and N. Donato, "Temperature effects on DC and small signal RF performance of AlGaAs/GaAs HEMTs," *Microelectron. Rel.*, vol. 46, no. 1, pp. 169–173, 2006.

[40] M. A. Alim, A. Z. Chowdhury, S. Islam, C. Gaquiere, and G. Crupi, "Temperature-sensitivity of two microwave HEMT devices: AlGaAs/GaAs vs. AlGaN/GaN heterostructures," *Electronics*, vol. 10, no. 9, p. 1115, 2021.

[41] J. Lu, Y. Wang, L. Ma, and Z. Yu, "A new small-signal modeling and extraction method in AlGaN/GaN HEMTs," *Solid-State Electron.*, vol. 52, no. 1, pp. 115–120, 2008, doi: 10.1016/j.sse.2007.07.009.